RSC Advances

PAPER

View Article Online
View Journal | View Issue

Cite this: *RSC Adv.*, 2023, **13**, 23669

Effect of ionic liquids on the microstructure and combustion performance of Shengli lignite

Xiaowei Hou, Hanyu Duan, Runxia He,* Huacong Zhou, Yanpeng Ban, Na Li, Keduan Zhi, Yinmin Song and Quansheng Liu*

To ensure the safe transportation and efficient utilisation of lignite, it is important to inhibit its spontaneous combustion. In this study, Shengli lignite (SL^+) was used as the research object and ionic liquids (ILs) were used to pretreat the lignite to investigate their effect on the combustion performance of lignite. On this basis, the relationship between the structure and combustion performance of lignite with different structures (heat treatment, oxidation) after ILs treatment was investigated. Results indicated that the combustion of lignite treated with ILs shifted towards higher temperatures. The most pronounced effect was observed in coal samples treated with [BMIM]Cl (1-butyl-3-methylimidazolium chloride), with the maximum combustion rate corresponding to a temperature increase of approximately 57 °C compared to that of the untreated lignite. For the heat-treated lignite, the temperature corresponding to the maximum combustion rate was approximately 38 °C higher than that of the untreated lignite. After [BMIM]Cl treatment, the combustion performance of the heat-treated lignite changed very slightly. In contrast, for oxidised lignite, the temperature corresponding to the maximum combustion rate decreased by approximately 54 °C compared with that of the untreated lignite and increased by approximately 135 °C after treatment with [BMIM]Cl. The characterisation results show that the content of aliphatic hydrogen and oxygen-containing functional groups decreased in the heat-treated lignite, while the content of hydroxyl and carboxyl groups increased in the oxidised lignite. The microstructure of the heat-treated lignite after [BMIM]Cl treatment changed slightly. In contrast, in the oxidised lignite after [BMIM]Cl treatment, the content of hydroxyl and carboxyl groups decreased, whereas the content of ether (C–O–) structures increased. The increased content of ether (C–O–) structures improved the stability of the coal samples. It is believed that the inhibition of lignite combustion is mainly attributed to the high stability of the ether (C–O–) structures. The kinetic analysis demonstrated that the ILs treatment increased the activation energy of lignite combustion.

Received 14th June 2023
Accepted 2nd August 2023

DOI: 10.1039/d3ra03976e

rsc.li/rsc-advances

1 Introduction

Coal remains the main energy source in many countries, such as China, India and the USA. As China is rich in coal but has limited oil and natural gas resources, China's energy sources are expected to still be dominated by coal in the future, with a large proportion of the reserves originating from low-order coal, such as lignite.[1,2] Lignite is a mixture of organic three-dimensional network macromolecules, inorganic minerals and various types of active groups.[3,4] Due to its low degree of coalification and high reactivity, lignite can be used for power generation and for the production of various products. However, its high moisture content, low calorific value and proneness to spontaneous combustion pose safety hazards during transportation and storage, significantly hindering its effective utilisation. Additionally, gases such as CO, CO_2, SO_2 and NO_x, which are produced by the spontaneous combustion of lignite, have adverse effects on the environment.[5] Therefore, inhibiting the spontaneous combustion of lignite is crucial.

The spontaneous combustion of lignite is a complex process involving physical and chemical reactions between the active functional groups in coal and oxygen. The different structural compositions of lignite, such as alkyl, aryl, carbonyl, carboxyl, hydroxyl and other functional groups, affect the reactivity and stability of coal in the air, some of which are more active in coal oxidation, triggering a series of exothermic reactions. Therefore, these functional groups mainly determine the spontaneous combustion tendency of coal.[6,7] With the increase in the coal rank, the microcrystalline structure can affect the spontaneous combustion tendency and low-temperature oxidation ability of coal.[8] The small molecule structures in the side chains of coal are easily oxidised, and the hydroxyl and carboxyl groups

College of Chemical Engineering, Inner Mongolia University of Technology, Inner Mongolia Key Laboratory of High-Value Functional Utilization of Low Rank Carbon Resources, Huhhot 010051, Inner Mongolia, China. E-mail: runxiahe@imut.edu.cn; liuqs@imut.edu.cn; Tel: +86 13664742350; +86 13664740405

are key factors the affect the spontaneous combustion of coal.[9,10] Acid treatment can increase the pore volume and porosity of coal, which enhances the adsorption of oxygen on coal and accelerates oxidation at low temperatures.[11] For example, heat treatment can considerably reduce the volatile content in lignite and start to remove oxygen-containing functional groups at approximately 300 °C.[12] Treatment with H_2O_2 can also break weak covalent bonds in lignite and introduce oxygen-containing functional groups.[13] This treatment method greatly affects the structure of lignite, thereby affecting its oxidation process, in which more active functional groups further trigger spontaneous combustion.

At present, various techniques have been reported to suppress the spontaneous combustion of coal, such as inertness, cooling and inhibition techniques.[14,15] Inert technology mainly dilutes or expels air in the space above coal the seam through the diffusion of inert gas or the expansion of inert foam, which reduces oxygen supply during combustion and minimises the frequency of coal–oxygen contact, thus inhibiting spontaneous combustion. However, this technology requires an airtight space, resulting in high costs.[16,17] Cooling technology mainly uses gel inhibitors and jet grouting to inhibit coal combustion. However, gel inhibitors release large amounts of ammonia during the gelation process, which poses a safety risk to industry personnel. Furthermore, most slurry inhibitors still have problems such as poor fluidity and blockage of transmission pipelines.[18,19] Inhibition technology has been widely promoted worldwide due to its simple process, wide source of raw materials and low cost.[20–22] It mainly uses inhibitors to accelerate the adsorption of water on the coal surface and prevent oxygen from contacting the active centre of the coal surface to inhibit the spontaneous combustion of lignite. For example, treating lignite with halogen salt inhibitors can increase the adsorbed water and retain it on the surface to prevent spontaneous combustion.[23] However, due to the fluidity of air and water, the inhibiting time of this inhibitor is not long, and continuous inhibition of spontaneous combustion has poor efficacy.[24] Sodium phosphate, ammonium salts, antioxidants and other inhibitors can be used to interact with the active groups on the lignite surface to reduce the number of active groups or inhibit free radical reactions. However, these inhibitors do not consider the changes in the functional groups in coal based on its structural diversity. Moreover, these inhibitors have the disadvantages of poor high-temperature resistance, easy loss and the potential to produce toxic and harmful gases.[25] Therefore, appropriate inhibitors should be selected to develop effective methods to reduce the spontaneous combustion of lignite.

Ionic liquids (ILs) are a type of green solvent with the characteristics of easy recovery, good solubility and high thermal stability. Additionally, ILs can be used to reduce the active groups in the molecular structure of coal, thereby inhibiting the oxidation of coal.[26,27] Some ILs can decompose the coal structure, or their functional groups can react with groups in the coal structure. For example, the oxygen-containing functional groups in $[AOEmim]^+$ and $[HOEmim]^+$ can form complexes with some groups in coal to form carboxyl groups.[28] Furthermore, quaternary ammonium ILs can react with hydrogen bonds and π-cations in dissolved asphaltene.[29] Zhang *et al.*[30] observed the variation law of hydrogen bonds during the low temperature oxidation of coal before and after the treatment of ILs ([EMIm]BF_4 and [BMIm]BF_4). They found that ILs have a certain inert effect on the reactivity of hydrogen bonds in coal. Imidazolium-based ILs can destroy active structures in lignite, particularly hydroxyl-conjugated hydrogen bonds and oxygen-containing functional groups, and increase the initial temperature of the exothermic oxidation reaction.[31,32] Additionally, imidazole ILs can promote the formation of –COOH in bituminous coal with good recyclability.[33,34] Deng *et al.*[35] noted that imidazole ILs can destroy the C=O structure in coal more effectively than ILs without imidazole, thereby reducing the thermal reactivity of coal. Furthermore, the length of the alkyl chain in imidazole ILs is proportional to imidazole ILs solubility.[36] For example, ILs with side chain $[BMIM]^+$ have better solubility than those with side chain $[AMIM]^+$. ILs with the same side chain and different anions exhibit different solubility in coal. For example, ILs with side chain $[BMIM]^+$ exhibit higher solubility of $[Cl]^-$ than $[BF_4]^-$.[37,38] Song *et al.*[39] treated Xinjiang lignite with four imidazole ILs of the same chain ($[BMIM]^+$). The results showed that compared with the other three ILs, [BMIM][BF_4] can destroy the hydroxyl functional groups in coal more effectively and achieve flame-retarding properties. Xie *et al.*[40] investigated the effect of a composite solvent composed of acid and ILs on the functional groups of coal. It was found that the content of hydroxyl groups on the surface of coal increased after treatment with sodium dodecyl sulphate and the content of aliphatic structures in coal was effectively reduced.

The above literature suggests that treatment with ILs can modify the content of active groups in coal, delay the oxidation of coal and increase the ignition temperature of coal. However, the relationship between specific organic structural changes in coal and combustion performance during ILs treatment is still unclear. Therefore, it is necessary to understand the relationship between the structural transformation characteristics of lignite treated with ILs and its combustion reaction performance, which is helpful in developing better methods to control the spontaneous combustion of lignite.

This study focuses on lignite and uses various ILs, such as 1-butyl-3-methylimidazolium chloride ([BMIM]Cl), 1-allyl-3-methylimidazolium chloride ([AMIM]Cl) and 1-butyl-3-methylimidazolium acetate ([BMIM]Ac), to pretreat lignite under the same conditions. Their effects on the combustion performance of lignite are then investigated. On this basis, this study investigates the relation between the structural and combustion performance of lignite with different structures (heat treatment, oxidation) after ILs treatment. Furthermore, the kinetics of the combustion of coal samples is analysed. The research results provide a reference for suppressing the spontaneous combustion of lignite and ensuring its safe and efficient use.

2 Experimental section

2.1 Experiment reagent

Air (O_2: 20.94%, N_2: 78.09%, Ar: 0.93% and CO_2: 0.033%) and nitrogen were obtained from Beijing Analytical Instrument Company. Hydrochloric acid (analytically pure, 38% wt%) was purchased from Tianjin Yongsheng Superfine Chemical Industry Co., Ltd. Hydrogen peroxide (analytically pure) was purchased from Tianjin FengChuan Chemical Reagent Technology Co., Ltd. The ILs (99.99%) were purchased from Lanzhou Aolike Chemical Co., Ltd. All chemical reagents were used directly without further purification.

2.2 Preparation of the coal samples

The experimental coal was obtained from the Shengli Coalfield in Xilingol, Inner Mongolia, and is referred to as Shengli lignite (SL). The SL was sieved and crushed to 0.075–0.150 mm, dried at 105 °C for 5 h and sealed and stored for future use.

Hydrochloric acid was used to remove minerals from SL. SL was mixed with hydrochloric acid (18.5%) in a ratio of 1 g to 10 mL and stirred at room temperature for 10 h. Then, the supernatant was filtered and washed with distilled water until the $AgNO_3$ test was negative for Cl^-. The resulting sample was dried at 105 °C for 4 h and labelled as SL^+.

The proximate and ultimate analyses of the samples are listed in Table 1. Compared with SL, SL after pickling (SL^+) has an ash content that is 65.8% lower, fixed carbon content increased and oxygen content decreased.

SL^+ was mixed with ILs [BMIM]Cl, [AMIM]Cl and [BMIM]Ac (see Table 2 for structural information) in a mass ratio of 1 : 2 and stirred for 8 h. Then, the sample was filtered and washed with distilled water until the filtrate was neutral. The coal samples were dried under vacuum at 80 °C for 48 h and cooled to room temperature. The resulting coal samples were labelled as SL^+-[BMIM]Cl, SL^+-[AMIM]Cl and SL^+-[BMIM]Ac.

For the preparation of the heat-treated coal samples, a certain amount of SL^+ was weighed and placed in a reaction tube. Under a nitrogen atmosphere, the coal samples were heated from room temperature to 150 °C at a heating rate of 3 °C min^{-1}, and a constant temperature was maintained for 1 h to remove moisture from the samples. Then, the temperature was increased to 220 °C at a heating rate of 10 °C min^{-1}. To prevent the termination temperature from being too high due to the rapid heating rate, the temperature was raised to the selected temperature at a heating rate of 3 °C min^{-1}. After cooling to room temperature, the coal samples were removed, weighed, sealed and stored for future use. The coal samples were labelled as SL^+-*T* (where *T* represents the selected temperature).

The oxidised coal samples were prepared through hydrogen peroxide oxidation.[41] The preparation process was as follows: SL^+ and hydrogen peroxide were mixed in a ratio of 1 g to 1 mL in an ice-water bath and stirred at a speed of 300 rpm for 12 h. Then, the sample was filtered and washed with distilled water until the filtrate was neutral, and the filter cake was dried in a vacuum drying oven at 60 °C for 15 h. The oxidised coal samples were sealed and stored for future use and labelled as SL^+-H_2O_2.

The SL^+-*T* and SL^+-H_2O_2 samples obtained earlier were treated with [BMIM]Cl using the same method described for treating SL^+, and the processed samples were labelled as SL^+-*T*-[BMIM]Cl and SL^+-H_2O_2-[BMIM]Cl, respectively.

Table 1 Proximate analysis and ultimate analyses of Shengli lignite[a]

	Proximate analysis (wt%)			Ultimate analysis (wt%, d)				
Samples	A_d	V_d	FC_d	C	H	N	S	O*
SL	11.81	42.05	46.14	60.46	3.60	0.79	1.37	33.78
SL^+	4.07	40.25	55.68	65.18	3.80	0.82	1.30	28.90

[a] d-dry basis; A-ash, V-volatile and Fc-fixed carbon; * by difference.

2.3 Characterisation of the coal samples

2.3.1 Fourier transform infrared spectrometer (FTIR). A Fourier transform infrared (FTIR) spectrometer (Nicolet NEXUS 670) was used to analyse the infrared spectrum of the coal samples. The samples were scanned at a resolution of 4 cm^{-1} in the range of 650–4000 cm^{-1}. The collected infrared spectral data were mapped and Gaussian fitting was performed to determine the changes in the main functional groups of lignite during the ILs treatment. Meanwhile, the parameters of the infrared spectrum were calculated using the peak area of the fitted curve, namely the aliphatic structure parameter $A_{(-CH_2-)}/A_{(-CH_3)}$ and the aromatic structure parameter H_{ar}/H_{al}.[42]

The aliphatic structural parameter $A_{(-CH_2-)}/A_{(-CH_3)}$ was used to characterise the length of the aliphatic chains and degree of branching aliphatic side-chains, which can be determined using eqn (1).[43,44]

$$A_{(-CH_2-)}/A_{(-CH_3)} = A_{(2927+2850)}/A_{(2957+2880)} \quad (1)$$

where $A_{(2927+2850)}$ and $A_{(2957+2880)}$ are the area of the –CH_2– and –CH_3 stretching vibration peaks, respectively. As the $A_{(-CH_2-)}/A_{(-CH_3)}$ ratio increases, the aliphatic chains of the aromatic rings increase. In contrast, a lower $A_{(-CH_2-)}/A_{(-CH_3)}$ ratio indicates a more compact structure between the aromatic rings.

The apparent aromaticity of coal was characterised by the parameter calculated using eqn (2).[45,46]

$$H_{ar}/H_{al} = A_{(900-700)}/A_{(3000-2800)} \quad (2)$$

where $A_{(900-700)}$ is the area in the 900–700 cm^{-1} range, which represents the content of aromatic hydrogen; $A_{(3000-2800)}$ is the area in the 3000–2800 cm^{-1} range, which represents the content of aliphatic hydrogen. As the H_{ar}/H_{al} ratio increases, the aromatic content and stability of the coal structure increase.

2.3.2 X-ray photoelectron spectroscopy (XPS). The chemical elements on the surface of the samples were characterised *via* X-ray photoelectron spectroscopy (XPS) (PHI-5400, Thermo-Fisher, USA). The vacuum degree was set to 3×10^{-7} Pa, while the power was set to 200 W. The scanning area was 300 × 300 μm, and the test data were corrected with C1s (284.6 eV) as the standard.

Table 2 Information on ionic liquids used in the experiment

Chemical name	Abbreviated name	Molecular formula	Structural formula
1-Butyl-3-methylimidazolium chloride	[BMIM]Cl	$C_8H_{15}N_2Cl$	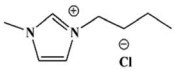
1-Allyl-3-methylimidazolium chlorides	[AMIM]Cl	$C_7H_{11}N_2Cl$	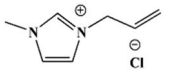
1-Butyl-3-methylimidazole acetate	[BMIM]Ac	$C_{10}H_{18}N_2O_2$	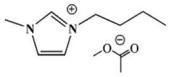

For the corrected XPS energy spectrum data, XPSPEAK 4.1 software was used to perform the peaking fitting of the XPS C1s spectrum of the coal samples to determine the changes in the content of carbon oxygen bonding structures of lignite during ILs treatment.

2.4 Combustion characteristics and kinetic analysis

A thermogravimetric analyser (China Hengjiu HCT-4) was used to test the combustion performance of the coal samples. The experimental steps were as follows: 15–20 mg of the coal samples were placed in an Al_2O_3 crucible and heated from room temperature to 700 °C at a heating rate of 10 °C min^{-1} in air atmosphere with a gas flow rate of 100 mL min^{-1}. The comprehensive combustion index S of the coal samples was calculated based on the thermogravimetric (TG) and derivative thermogravimetric (DTG) curves.[47] S reflects the combustion performance of the coal samples, and a higher S value indicates better combustion performance. The calculation formula for S is as follows:

$$S = \frac{(\mathrm{d}x/\mathrm{d}y)_{\max}(\mathrm{d}x/\mathrm{d}t)_{\mathrm{mean}}}{T_i^2 T_b} \quad (3)$$

where $(\mathrm{d}x/\mathrm{d}t)_{\max}$ is the maximum mass loss rate, $(\mathrm{d}x/\mathrm{d}t)_{\mathrm{mean}}$ is the average mass loss rate, T_i is the ignition temperature and T_b is the burnout temperature.

The kinetic calculation of the coal samples in the combustion process was performed using the Coats–Redfern integral method,[48,49] which is widely used in the determination of lignite thermodynamics. The apparent activation energy E of the combustion reaction calculated using this method was used to measure the reactivity of the coal samples. The kinetic equation of the combustion process can be expressed as follows:

$$\frac{\mathrm{d}\alpha}{\mathrm{d}t} = A\exp\left(-\frac{E}{RT}\right)(1-\alpha)^n \quad (4)$$

In the non-isothermal combustion experiment, assuming that the heating rate of the reaction is β, $T = T_0 + \beta t$, where T_0 is the starting temperature of the experiment and α is the conversion rate. To facilitate comparison and calculation, the combustion reaction is considered as a first-order reaction ($n = 1$). After integral transformation, the following equation can be obtained:

$$\ln\left[\frac{-\ln(1-\alpha)}{T^2}\right] = \ln\frac{AR}{\beta E} - \frac{E}{RT} \quad (5)$$

The apparent activation energy E and finger front factor A can be calculated by fitting the slope and intercept of the line obtained by plotting $\ln[-\ln(1-\alpha)/T^2]$ as the vertical coordinate and $1/T$ as the horizontal coordinate.

3 Results and discussion

3.1 ILs treatment of lignite

3.1.1 Combustion characteristics. Fig. 1 presents the combustion performance curves of the SL^+ and coal samples treated with different ILs. It can be seen that the weight loss at temperatures below 200 °C was caused by the evaporation of water in the coal samples and the desorption of small-molecule gases,[50] with SL^+ exhibiting the largest weight loss. The weight loss of the coal samples after ILs treatment was considerably reduced, with coal samples treated with [BMIM]Cl exhibiting the lowest weight loss. The weight loss after 200 °C was caused by the combustion of volatiles and fixed carbon in the coal samples. The weight loss rate of the SL^+ and coal samples treated with [BMIM]Ac was higher, while that of the coal samples treated with [BMIM]Cl and [AMIM]Cl was lower. In the main combustion zone of 300–600 °C, the combustion rate of SL^+ was the highest, while that of the coal samples treated with [BMIM]Cl was the lowest. The combustion rates of the other treated coal samples were between those of SL^+ and the samples treated with [BMIM]Cl. The DTG curves demonstrated that compared with that of SL^+, the maximum combustion rate of the ILs-treated coal samples decreased to varying degrees, and the temperature corresponding to the maximum combustion rate increased to varying degrees. The temperature corresponding to the maximum combustion rate of the coal samples treated with [BMIM]Cl was increased by approximately 57 °C, indicating that ILs treatment inhibited the combustion of the coal samples. Based on the above results, it could be seen that the inhibition effect of ILs on the combustion reaction of lignite was mainly attributed to the interaction of the ILs with the active functional groups in lignite.[26,35] Moreover, the difference in the inhibition performance of different ILs on the

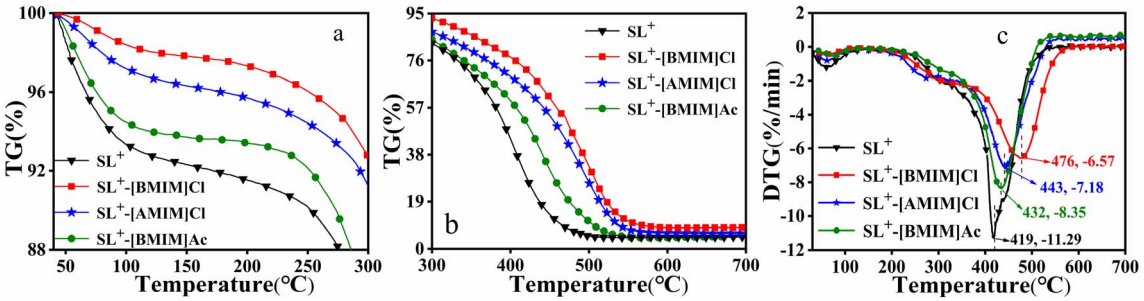

Fig. 1 Combustion performance curves of SL^+ and coal samples treated with different ILs: (a) TG (25–300 °C); (b) TG (300–700 °C); (c) DTG.

combustion reaction of lignite was ascribed to the length of its side chain and the types of anions.[28,33]

The combustion parameters calculated based on the combustion performance curves are presented in Table 3. Compared with SL^+, the ILs-treated coal samples exhibited a significant decrease in the combustion rate, an increase in the ignition temperature T_i and temperature corresponding to the maximum combustion rate T_m, and a decrease in the combustion index S. These results indicate that ILs treatment can improve the stability of coal samples. The flame retardant effect of the different ILs followed the order [BMIM]Cl > [AMIM]Cl > [BMIM]Ac. When anion (Cl^-) was the same, the flame retardant effect of side chain $[BMIM]^+$ was superior to that of $[AMIM]^+$. When the cationic side chain ($[BMIM]^+$) was the same, the inhibitory effect of anion Cl^- was superior to that of Ac^-.

3.1.2 Characterisation analysis

3.1.2.1 FTIR analysis. To understand the changes in the functional groups of the coal samples treated with ILs, the FTIR spectra of the above samples were analysed. Fig. 2 presents the FTIR spectra of SL^+ and coal samples treated with different ILs. It can be seen from Fig. 2(a) that the infrared spectra of SL^+ and the ILs-treated coal samples maintained the same shape and peak position, indicating that the main functional groups of the coal samples did not change significantly after ILs treatment. However, some characteristic peaks of the coal samples after ILs treatment, such as the characteristic peak intensity of hydroxyl groups with a wave number of approximately 3400 cm^{-1} and the $-CH_2-$ and $-CH_3$ groups in the range of 3000–2800 cm^{-1}, were weakened. Moreover, the ILs-treated coal samples exhibited obvious ether (C–O–) structural characteristic peaks at a wave number of 1160 cm^{-1}.

To compare the differences in the microstructure of coal samples treated with different ILs, the FTIR spectra of the coal samples were divided into three regions hydrogen bond, aliphatic hydrogen and oxygen-containing functional groups for Gaussian fitting.[51] The fitting diagram is presented in Fig. 2(b), while the fitting results are presented in Fig. 2(c) and (d). Fig. 2(c) displays the content of each oxygen-containing group calculated by fitting the peak area of the curve. It can be observed that the content of hydroxyl and carboxyl groups in the coal samples decreased to a certain extent after ILs treatment, while the content of ether (C–O–) structures increased, indicating that ILs treatment promoted the conversion of hydroxyl or carboxyl groups to ether structures. [BMIM]Cl played a more significant role in promoting the formation of ether structures. Fig. 2(d) displays a fitting parameter diagram. The aliphatic side chain length $A_{(-CH_2-)}/A_{(-CH_3)}$ of the ILs-treated coal samples decreased, and the ratio of aromatic hydrogen to aliphatic hydrogen H_{ar}/H_{al} increased, indicating that ILs treatment reduced the content of aliphatic C–H in the coal samples, increased the content of aromatic hydrogen and improved the structural stability of the coal samples. When the anion (Cl^-) was the same, $[BMIM]^+$ promoted the formation of ether structures in the coal samples more effectively than $[AMIM]^+$, which was related to the length of the side chains.[52] When the cationic side chain ($[BMIM]^+$) was the same, ILs containing Cl^- promoted the formation of ether structures in the coal samples more effectively than ILs containing Ac^-, possibly due to the smaller size of Cl^- and its stronger electronegativity, allowing it to be more efficiently distributed in the pores of coal and firmly attached to the surface of coal to prevent coal combustion.[53,54]

Table 3 Combustion parameters of SL^+ and the coal samples treated with different ILs[a]

Samples	T_i (°C)	T_m (°C)	DTG_{max} (% min^{-1})	$S \times 10^{-7}$ (%^{2} min^{-2} °C^{-3})
SL^+	353	419	−11.29	2.66
SL^+-[BMIM]Cl	393	476	−6.57	1.32
SL^+-[AMIM]Cl	378	443	−7.18	1.46
SL^+-[BMIM]Ac	368	432	−8.35	2.11

[a] T_i, ignition temperature; T_m, temperature corresponding to the maximum combustion rate; DTG_{max}, maximum weight loss rate; S, combustion index.

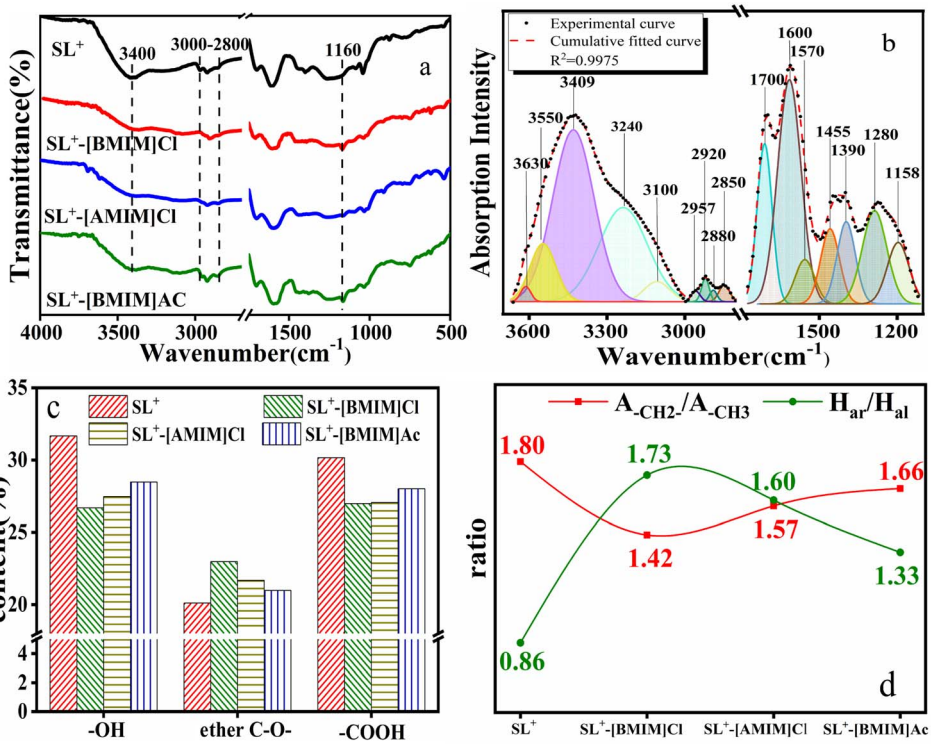

Fig. 2 FTIR spectra of SL^+ and the coal samples treated with different ILs: (a) full spectrum; (b) fitting diagram; (c) content of oxygen-containing groups; (d) fitting parameters.

3.1.2.2 XPS analysis. Fig. 3 presents the C1s spectra of SL^+ and the coal samples treated with different ILs. To obtain detailed information on the surface of the coal samples treated with SL^+ and ILs, XPSPEAK 4.1 software was used to perform peak fitting on the C1s spectra of the coal samples. According to the literature,[55,56] there are five forms of C1s on the surface of coal samples: aromatic units and their substituted alkanes C–C/C–H (284.6 eV), vacancy defects on functional groups C*–C* (285.3 eV), ether-based C–O– (286.4 eV), carbonyl-based C=O (287.6 eV) and carboxyl-based COO– (289.1 eV). Fig. 3(b) presents a fitting schematic diagram using SL^+ as an example, while Fig. 3(c) displays the fitting results of all surface C1s of coal samples. Fig. 3(c) demonstrates that the content of C–C/C–H and COO– on the surface of the coal samples after ILs treatment decreased, while the C–O– content increased, especially in SL^+-[BMIM]Cl, where the C–O– content had the largest increase. Because C–O– is a stable carbon–oxygen structure in coal,[57] the content of C–O– in coal samples treated with [BMIM]Cl was relatively high, indicating that [BMIM]Cl more effectively promoted the formation of ether structures. This finding is consistent with the FTIR characterisation results and the combustion performance of the coal samples.

3.2 Treatment of lignite with different structures using ILs

The results presented in Section 3.1 indicate that ILs can alter the microstructure of lignite by promoting the conversion of hydroxyl and carboxyl groups into ether-like structures, thereby reducing the content of active groups and inhibiting the combustion of lignite. To further investigate the relation between the microstructural changes and combustion performance of lignite treated with ILs, different structures of lignite (heat-treated at 300 °C [SL^+-300] and treated by H_2O_2 oxidation [SL^+-H_2O_2]) were examined.

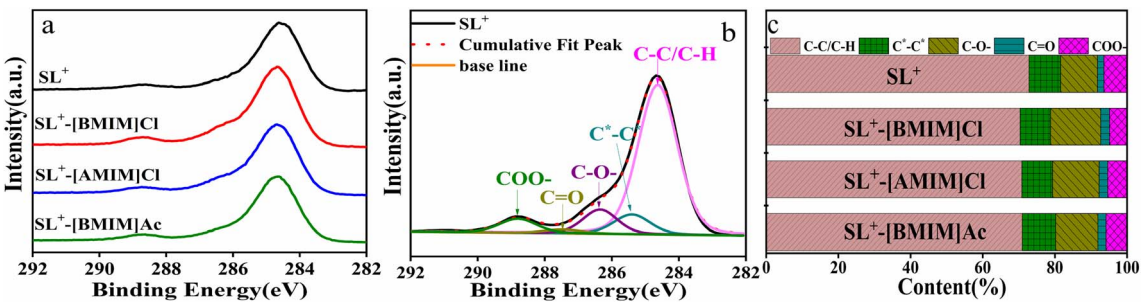

Fig. 3 XPS spectra of SL^+ and the coal samples treated with different ILs: (a) C1s spectra; (b) fitting diagram; (c) fitting results.

The treatment was performed using [BMIM]Cl, which had a stronger inhibition effect, and the combustion performance of the [BMIM]Cl-treated lignite was investigated using a thermogravimetric analyser. The microstructural changes of the [BMIM]Cl-treated lignite were analysed using characterisation methods, and the mechanism of inhibiting the spontaneous combustion of lignite was analysed based on changes in the kinetic parameters during the combustion process.

3.2.1 Combustion characteristics. Fig. 4 presents the combustion performance curves of SL^+-300, SL^+-H_2O_2 and their [BMIM]Cl-treated coal samples. As illustrated in Fig. 4(a) and (b), heat treatment at 300 °C caused the combustion curve of SL^+ to shift towards higher temperatures, with the temperature corresponding to its maximum combustion rate being higher than that of SL^+ by approximately 38 °C. After treatment with [BMIM]Cl, the temperature corresponding to the maximum combustion rate of SL^+-300 did not change significantly compared to that of the heat-treated coal samples. In contrast, the H_2O_2 oxidation treatment caused the combustion curve of the coal samples to shift towards lower temperatures, and the temperature corresponding to its maximum combustion rate was approximately 54 °C lower than that of SL^+. After [BMIM]Cl treatment, the temperature corresponding to SL^+-H_2O_2-[BMIM]Cl maximum combustion rate was approximately 81 °C and 135 °C higher than that of SL^+ and SL^+-H_2O_2, respectively. Based on the above results, it could be seen that due to the structural differences between the heat-treated and oxidised coal samples, the combustion reaction performances of the two coal samples was significantly different. In the ILs treatment process, the [BMIM]Cl had different effects on the active functional groups of the two lignite treated coals, resulting in a large difference in their inhibition effects of the combustion reaction, where the combustion reaction performance of oxidized coal samples was considerably inhibited.

The combustion parameters calculated based on the curve in Fig. 4 are presented in Fig. 5. The results in Fig. 5(a) indicate that the T_i of the coal sample heat-treated at 300 °C was higher than that of SL^+, and the T_m corresponding to the maximum combustion rate was higher than that of SL^+. Furthermore, the weight loss rate decreased, which indicated that the combustible active structures in the coal samples decreased after heat treatment. The characteristic temperature changes of the coal samples after [BMIM]Cl treatment were not significant. Fig. 5(b) indicates that the T_i and T_m of the coal samples treated with H_2O_2 were much lower than those of SL^+, indicating that the combustible active structures in the coal sample increased after oxidation. After [BMIM]Cl treatment, the characteristic temperatures of the coal samples were significantly increased and the weight loss rate was greatly reduced, which illustrated the considerable reduction in the flammable active structure in the oxidised coal samples. The variation in the combustion index S in Fig. 5(b) further illustrates the differences in the combustion performance of lignite with different structures treated with [BMIM]Cl.

3.2.2 FTIR analysis. Fig. 6 presents the FTIR spectra of SL^+-300, SL^+-H_2O_2 and their [BMIM]Cl-treated coal samples. This figure demonstrates that the hydroxyl and carboxyl groups of the SL^+-300 coal samples as well as the absorption peak intensities of –CH_2– and –CH_3 weakened. However, after treatment with [BMIM]Cl, the functional groups in the coal sample exhibited little change. The absorption peaks of the hydroxyl strength of the SL^+-H_2O_2 coal sample slightly increased, while the absorption peaks of strength of –CH_2– and –CH_3 decreased, and the absorption peaks of strength of carboxyl at 1700 cm^{-1} increased. The absorption peaks of hydroxyl, –CH_2– and –CH_3 decreased after [BMIM]Cl treatment. Although the carboxyl absorption peak did not appear to change considerably, a distinct characteristic peak of the ether structure C–O– appeared at a wave number of 1160 cm^{-1}. The

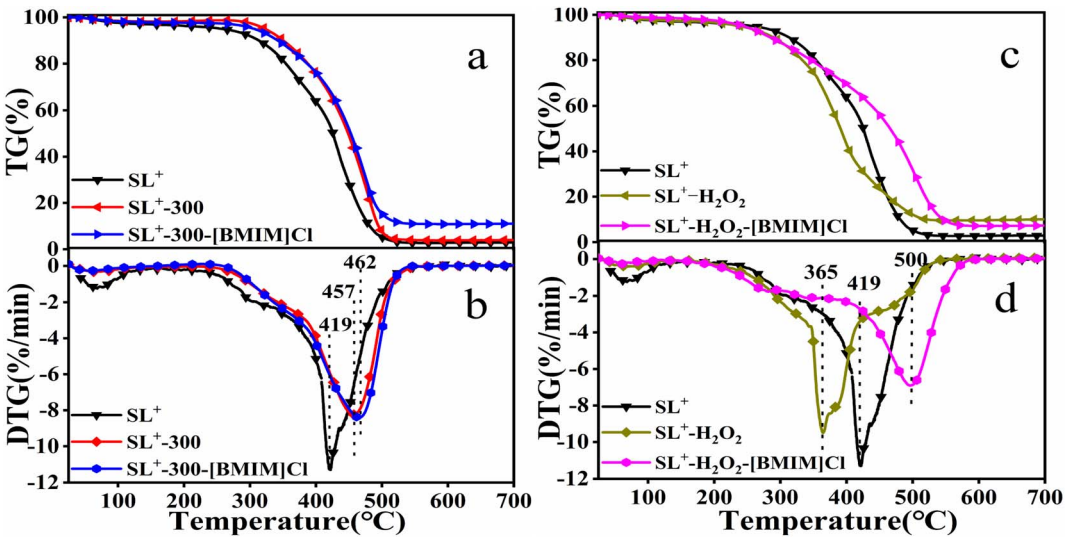

Fig. 4 TG/DTG curves of lignite with different structures before and after treatment with [BMIM]Cl: (a and b) heat treatment; (c and d) oxidation treatment.

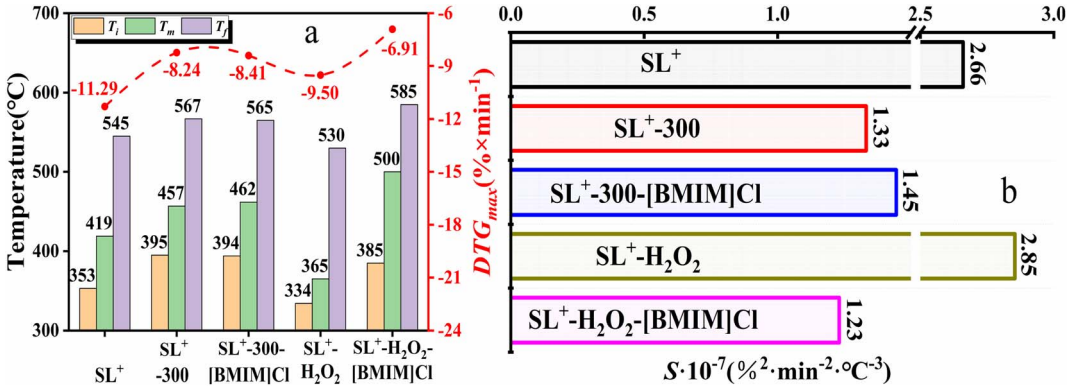

Fig. 5 Combustion parameters of lignite with different structures before and after [BMIM]Cl treatment.

appearance of the ether structure increased the stability of the coal samples, making them more difficult to fracture during their oxidation process, leading to an increase in the temperature corresponding to the maximum combustion rate.

The FTIR spectra of lignite with different structures before and after [BMIM]Cl treatment were fit, and the content of each oxygen-containing group and the fitting parameters were obtained, as illustrated in Fig. 6(b) and (c), respectively. As illustrated in Fig. 6, the content of hydroxyl and carboxyl groups in the coal sample decreased after heat treatment, indicating that heat treatment removed some –OH and caused the decomposition of some –COOH. However, after H_2O_2 oxidation treatment, the content of hydroxyl and carboxyl groups increased, which was due to the fact that H_2O_2 oxidised some of the aliphatic side chains directly connected to the aromatic ring. After treatment with [BMIM]Cl, the content of various functional groups in the heat-treated coal samples did not change considerably, whereas the content of the hydroxyl and carboxyl groups in the H_2O_2-treated coal samples decreased, indicating that [BMIM]Cl treatment reduced the content of oxygen-containing groups in the coal. As the content of active groups in the coal samples of heat-treated was extremely less, the [BMIM]Cl treatment had less influence on the groups in the coal samples. In contrast, as the content of active groups in the oxidised coal samples increased, [BMIM]Cl treatment had a stronger influence on the active groups in the coal samples and the content of active groups was considerably reduced.

The content of ether (C–O–) structures increased slightly in the heat-treated coal samples, whereas it decreased in the oxidised coal samples. After [BMIM]Cl treatment, there was no significant change in the content of ether (C–O–) structures in the heat-treated coal samples; however, there was a significant increase in the content of ether (C–O–) structures in the oxidised coal samples. This indicates that [BMIM]Cl promoted the formation of ether (C–O–) structures in the oxidised coal samples, which in turn increased the stability of the coal samples. The above results indicate that the content of ether (C–O–) structures in coal samples treated with [BMIM]Cl was closely related to their structure. Oxidised coal samples contained more oxygen-containing functional groups, while heat-treated coal samples contained fewer oxygen-containing functional groups. Different results were obtained for SL$^+$-H_2O_2 and SL$^+$-300 after [BMIM]Cl treatment. Furthermore, treatment with [BMIM]Cl promoted the conversion of hydroxyl and carboxyl groups into ether (C–O–) structures.

Fig. 6(c) indicates that for the heat-treated coal samples, $A_{(-CH_2-)}/A_{(-CH_3)}$ decreased while H_{ar}/H_{al} increased. For the oxidised coal samples, $A_{(-CH_2-)}/A_{(-CH_3)}$ also decreased while H_{ar}/H_{al} slightly decreased. After treatment with [BMIM]Cl, there was little change in $A_{(-CH_2-)}/A_{(-CH3)}$ and H_{ar}/H_{al} of the heat-treated coal samples. However, for the oxidised coal samples, $A_{(-CH_2-)}$/

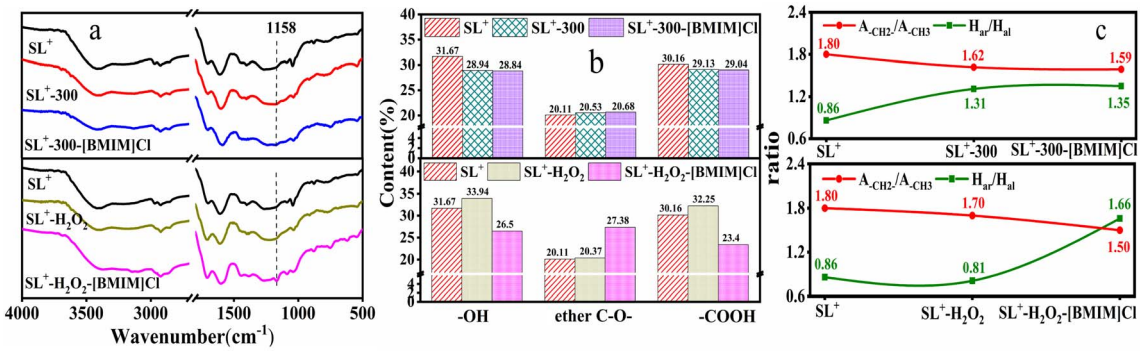

Fig. 6 FTIR spectra of lignite with different structures before and after [BMIM]Cl treatment: (a) full spectrum diagram; (b) oxygen-containing group content; (c) fitting parameters.

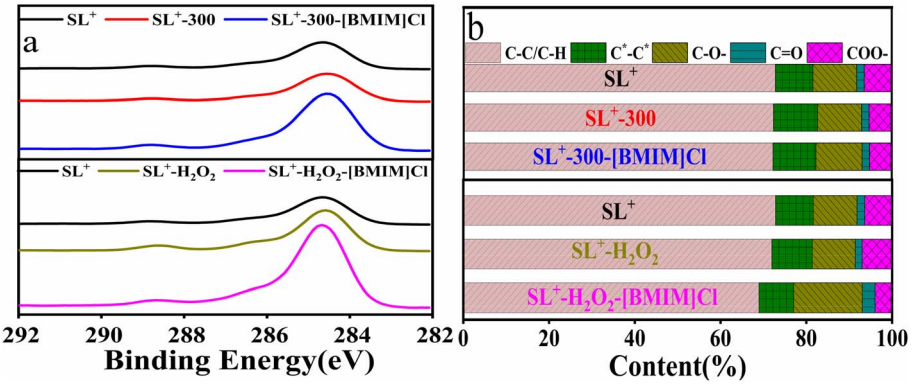

Fig. 7 XPS spectra of lignite with different structures before and after treatment with [BMIM]Cl: (a) C1s spectra; (b) fitting results.

$A_{(-CH_3)}$ slightly decreased while H_{ar}/H_{al} significantly increased, indicating that ILs treatment increased the content of aromatic hydrogen and enhanced the stability of the coal.

3.2.3 XPS analysis. Fig. 7(a) and (b) present the XPS C1s spectra and fitting results, respectively, of SL^+-300, SL^+-H_2O_2 and the coal samples treated with [BMIM]Cl. As illustrated in the figure, compared with SL^+, SL^+-300 exhibited a decrease in the content of carboxyl COO– and an increase in the content of ether (C–O–) structures, indicating that heat treatment improved the stability of the coal samples. In SL^+-H_2O_2, the content of carboxyl COO– increased, whereas that of ether (C–O–) structures decreased, indicating that oxidation treatment increased the content of active functional groups in the coal samples. After treatment with [BMIM]Cl, the content of carbon groups in the heat-treated coal samples remained basically constant. In contrast, in the oxidised coal samples, the COO– content decreased while the content of ether (C–O–) structures increased, suggesting that the stability of the oxidised coal samples was greatly improved by treatment with [BMIM]Cl. In oxidised coal samples treated with [BMIM]Cl, the maximum combustion rate occurred at a temperature approximately 135 °C higher than that of the oxidised coal samples.

In summary, the microstructural changes of coal samples with different structures during [BMIM]Cl treatment were closely related to the amount of –OH and COO– content in the coal. It is believed that [BMIM]Cl can convert some –OH and COO– in coal into ether (C–O–) structures.

3.2.4 Kinetic analysis. Fig. 8 presented the linear fit of the coal samples to the combustion stage (300–600 °C) obtained using the Coats–Redfern integration method. The correlation coefficients of the fitted curves for the coal samples were all within the range of 0.991–0.997. The kinetic parameters of the coal samples calculated on the basis of Fig. 8 are presented in Table 4. Compared to lignite, the heat-treated coal samples had a higher activation energy, while the oxidised coal samples had a lower activation energy, indicating a significant difference in the combustion performance of lignite with different structures. After [BMIM]Cl treatment, the activation energy of the heat-treated coal samples did not change considerably, whereas that of the oxidised coal samples increased considerably, which is consistent with the results presented in Fig. 4 and 5.

3.2.5 Mechanism analysis. The above results indicate that the formation of ether-like (C–O–) structures increased the stability of lignite and inhibited its combustion. Lignite treated with different ILs forms an ether (C–O–) structure, which can improve the stability of lignite and inhibit its combustion of lignite to varying degrees. The order of the inhibition effect is as follows: [BMIM]Cl > [AMIM]Cl > [BMIM]Ac. On this basis, [BMIM]Cl was further used to treat lignite with different structures (heat treatment, oxidation treatment). Because the heat-treated coal sample contained fewer oxygen containing functional groups and the oxidised coal

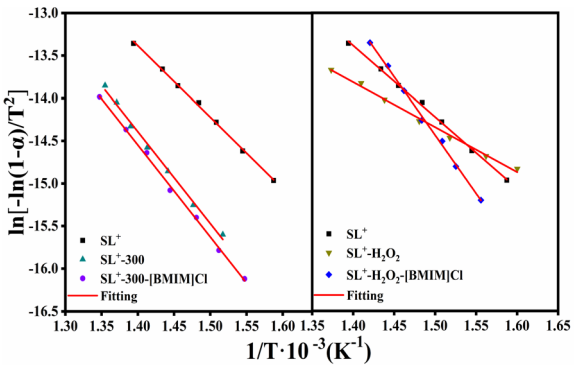

Fig. 8 Linear fitting diagram of the coal samples obtained using the Coats–Redfern integration method.

Table 4 Kinetic parameters of lignite with different structures before and after treatment with [BMIM]Cl

Samples	Temperature range (°C)	E (kJ mol^{-1})	A (min^{-1})	R^2
SL^+	391–456	69.79	1.64×10^4	0.997
SL^+-300	385–464	89.71	2.19×10^5	0.991
SL^+-300-[BMIM]Cl	388–465	89.82	1.93×10^5	0.993
SL^+-H_2O_2	372–442	43.83	8.50×10	0.995
SL^+-H_2O_2-[BMIM]Cl	398–486	114.08	6.43×10^7	0.992

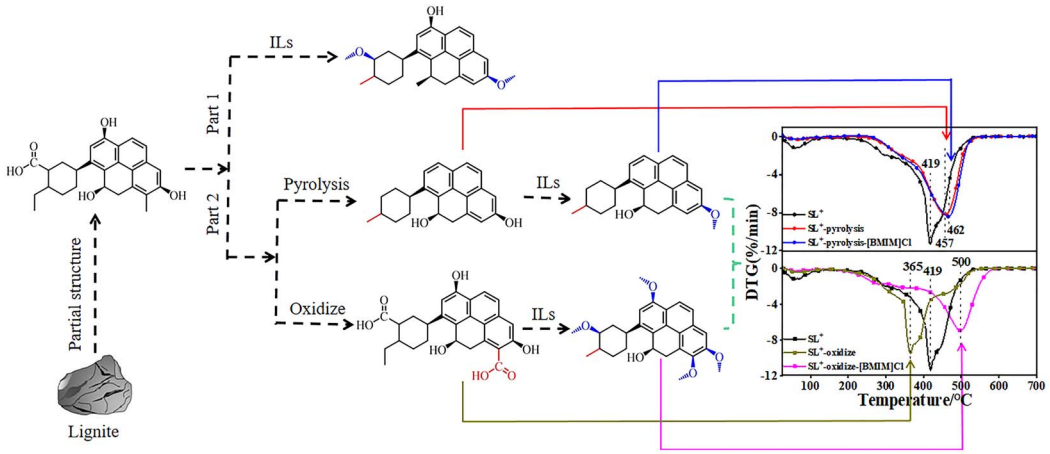

Fig. 9 Relation between the structure and combustion performance of Shengli lignite treated with ILs.

sample contained more oxygen containing functional groups, the [BMIM]Cl treatment process had different effects on the structure and combustion reaction performance of both types of samples, with a lesser effect on the heat-treated coal samples and a greater effect on the oxidised coal samples. Based on the results of this study and the complex structure of lignite samples, a possible correlation between the combustion performance and structure of lignite treated with ILs was proposed, as illustrated in Fig. 9. The relative amount of ether (C–O–) structures affected the inhibition of lignite combustion. The heat-treated coal samples contained fewer oxygen-containing functional groups, and their structures did not change significantly after ILs treatment. In contrast, oxidised coal samples contained more oxygen-containing functional groups, and more ether (C–O–) structures were formed after ILs treatment. The stability of the ether (C–O–) structures increased the temperature corresponding to the maximum combustion rate of lignite.

4 Conclusions

The effect of ILs treatment on the microstructure and combustion performance of SL^+ was investigated, and the following conclusions were drawn:

(1) Treatment with ILs shifted the combustion temperature of lignite towards higher temperature, and the effect of [BMIM]Cl treatment was more pronounced. The temperature corresponding to the maximum combustion rate was approximately 57 °C higher than that of the untreated lignite. [BMIM]Cl had little effect on the combustion reactivity of the heat-treated lignite but had a significant effect on the combustion reactivity of oxidised lignite.

(2) ILs treatment promoted the transformation of hydroxyl, carboxyl and other oxygen-containing functional groups in lignite to ether (C–O–) structures, and the increase in the content of ether (C–O–) structures improved the stability of the coal sample, hence, the temperature corresponding to the maximum combustion reaction rate of lignite moved to the high temperature region.

(3) The oxygen-containing functional groups such as hydroxyl and carboxyl groups in heat treated lignite decreased, whereas those in oxidised lignite increased. [BMIM]Cl treatment significantly increased the content of ether (C–O–) structures in oxidised lignite, which improved its stability.

The results of this study have practical significance for inhibiting the spontaneous combustion of lignite in real situations and thereby promoting its safe and effective utilisation.

Conflicts of interest

There are no conflicts to declare.

Acknowledgements

The authors greatly acknowledge the financial support from the National Natural Science Foundation of China (21566028, 21968021), Science and Technology Plan Project of Inner Mongolia (2020GG0289), and Natural Science Foundation of Inner Mongolia (2019MS02025, 2020MS02023).

References

1 M. Z. Khan, D. H. Chun, J. Yoo, S. D. Kim, Y. J. Rhim, H. K. Choi, J. Lim, S. Lee and A. Rifella, Evaluation of the effect of a palm acid oil coating on upgrading low rank coal, *RSC Adv.*, 2015, **5**, 63955–63963, DOI: **10.1039/c5ra08994h**.

2 G. Cheng, Z. Li, Z. Ma, Y. Cao, L. Sun and Z. Jiang, Optimization of collector and its action mechanism in lignite flotation, *Powder Technol.*, 2019, **345**, 182–189, DOI: **10.1016/j.powtec.2019.01.011**.

3 B. Zhang and Y. L. Chen, Particle size effect on pore structure characteristics of lignite determined *via* low-temperature nitrogen adsorption, *J. Nat. Gas Sci. Eng.*, 2020, **84**, 103633, DOI: **10.1016/j.jngse.2020.103633**.

4 F. Wei, J. Liao, L. Chang, Y. Han and W. Bao, Transformation of functional groups during lignite heat-treatment and its effects on moisture re-adsorption properties, *Fuel Process.*

Technol., 2019, **192**, 210–219, DOI: 10.1016/j.fuproc.2019.04.028.

5 J. Pallares, C. Herce, C. Bartolome and B. Pena, Investigation on co-firing of coal mine waste residues in pulverized coal combustion systems, *Energy*, 2017, **140**, 58–68, DOI: 10.1016/j.energy.2017.07.174.

6 Z. H. Yan, J. M. Chen, R. X. He, N. Li, H. C. Zhou, Y. M. Song, Y. P. Ban, K. D. Zhi, Y. Y. Teng and Q. S. Liu, Suppression of crosslinking combination of carboxyl functional groups with NaOH on combustion performance of Shengli lignite, *Fuel*, 2018, **227**, 13–20, DOI: 10.1016/j.fuel.2018.04.058.

7 Z. H. Yan, D. D. Wang, R. X. He, N. Li, H. C. Zhou, Y. F. Wang, Y. M. Song, K. D. Zhi, Y. Y. Teng and Q. S. Liu, Microstructural characteristics of Shengli lignite during low-temperature oxidation and promotion effect of iron species, *Fuel*, 2019, **255**, 115830.1–115830.9, DOI: 10.1016/j.fuel.2019.115830.

8 G. L. Dai, Research on microcrystalline structure change regularity in the coal low temperature oxidation process, *J. China Coal Soc.*, 2011, **36**, 322–325, DOI: 10.13225/j.cnki.jccs.2011.02.018.

9 J. R. Wang and C. B. Deng, The spontaneous combustion theory of coal microcosmic structure and component differences in quantity and quality, *J. China Coal Soc.*, 2007, **12**, 1291–1296, DOI: 10.3321/j.issn:0253-9993.2007.12.012.

10 X. Qi, D. Wang, H. Xin and G. Qi, An *in situ* testing method for analyzing the changes of active groups in coal oxidation at low temperatures, *Spectrosc. Lett.*, 2014, **47**, 495–503, DOI: 10.1080/00387010.2013.817433.

11 Y. Y. Wang, F. D. Mei and S. Xue, Comparative analysis of microstructure evolution and oxidation performance of acid-treated lignite, *Fuel Process. Technol.*, 2021, **215**, 106750, DOI: 10.1016/j.fuproc.2021.106750.

12 G. Da la Puente, M. J. Iglesias, E. Fuente and J. J. Pis, Changes in the structure of coals of different rank due to oxidation effects on pyrolysis behaviour, *J. Anal. Appl. Pyrolysis*, 1998, **47**, 33–42, DOI: 10.1016/S0165-2370(98)00087-4.

13 K. Mae, T. Maki, J. Araki and K. Miura, Extraction of low-rank coals oxidized with hydrogen peroxide in conventionally used solvents at room temperature, *Energy Fuels*, 1997, **11**, 825–831, DOI: 10.1021/ef960225o.

14 J. Deng, Y. Xiao, Q. W. Li, J. H. Lu and H. Wen, Experimental studies of spontaneous combustion and anaerobic cooling of coal, *Fuel*, 2015, **157**, 261–269, DOI: 10.1016/j.fuel.2015.04.063.

15 D. M. Wang, G. L. Dou, X. X. Zhong, H. H. Xin and B. T. Qin, An experimental approach to selecting chemical inhibitors to retard the spontaneous combustion of coal, *Fuel*, 2014, **117**, 218–223, DOI: 10.1016/j.fuel.2013.09.070.

16 J. Deng, Y. Yang, Y. N. Zhang, B. Liu and C. M. Shu, Inhibiting effects of three commercial inhibitors in spontaneous coal combustion, *Energy*, 2018, **160**, 1174–1185, DOI: 10.1016/j.energy.2018.07.040.

17 W. B. Zhao, H. S. Cao, X. Y. Shi, J. F. Wang, W. Z. Du and R. Z. Li, Study on Regional Distribution of Spontaneous Combustion in Goaf of Deep Inclined Working Face and Effect of Low Temperature Inert Gas Injection, *Combust. Sci. Technol.*, 2022, 1–21, DOI: 10.1080/00102202.2022.2150077.

18 G. J. Zhi, R. Xie, R. G. Yang, J. Q. Cui, X. Y. An and Y. L. Zhang, Study on the Preparation of Montmorillonite-Type Multiple Network Composite Gel for Coal Spontaneous Combustion and Its Firefighting Mechanism, *ACS Omega*, 2023, **8**(11), 10493–10502, DOI: 10.1021/acsomega.3c00138.

19 M. G. Yu, N. Yang, Z. Y. Liu, H. T. Li, L. Wang, M. Q. Wu, J. Li and Y. Y. Yu, Experimental preparation and mechanism analysis of a neotype composite gel for coal spontaneous combustion prevention and coal-fire extinguishment, *Fuel*, 2023, **339**, 127448, DOI: 10.1016/j.fuel.2023.127448.

20 H. Shao, H. Hu, Q. Z. Lu, S. G. Jing, X. D. Peim and Z. Y. Wu, Experimental Study on Water Retention and Flame Retardancy of Environmental Protection Slurry of Film Coated Gasification Slag, *Combust. Sci. Technol.*, 2023, 1–21, DOI: 10.1080/00102202.2023.2168539.

21 X. C. Hu, X. J. Zhu and Z. Q. Sun, Fireproof performance of the intumescent fire retardant coatings with layered double hydroxides additives, *Constr. Build. Mater.*, 2020, **256**, 119445, DOI: 10.1016/j.conbuildmat.2020.119445.

22 J. H. Li, Z. H. Li, C. J. Wang, Y. L. Yang and X. Y. Zhang, Experimental study on the inhibitory effect of ethylenediaminetetraacetic acid (EDTA) on coal spontaneous combustion, *Fuel Process. Technol.*, 2018, **178**, 312–321, DOI: 10.1016/j.fuproc.2018.06.007.

23 Y. B. Tang, Experimental investigation of applying $MgCl_2$ and phosphates to synergistically inhibit the spontaneous combustion of coal, *J. Energy Inst.*, 2018, **91**, 639–645, DOI: 10.1016/j.joei.2017.06.006.

24 Y. J. Wang, Y. F. Zhao, R. X. He, Z. H. Yan, X. M. Li, H. C. Zhou, N. Li, K. D. Zhi, Y. M. Song, Y. Y. Teng and Q. S. Liu, Effects of Water-Soluble Sodium Compounds on the Microstructure and Combustion Performance of Shengli Lignite, *ACS Omega*, 2021, **6**, 24848–24858, DOI: 10.1021/acsomega.1c03695.

25 J. Pallares, C. Herce, C. Bartolome and B. Pena, Investigation on co-firing of coal mine waste residues in pulverized coal combustion systems, *Energy*, 2017, **140**, 58–68, DOI: 10.1016/j.energy.2017.07.174.

26 C. B. Kirtikumar and M. B. Bhalchandra, Factors governing dissolution process of lignocellulosic biomass in ionic liquid: Current status, overview and challenges, *Bioresour. Technol.*, 2015, **178**, 2–18, DOI: 10.1016/j.biortech.2014.09.138.

27 N. Pulati, M. Sobkowiak, J. P. Mathews and P. Painter, Low-temperature treatment of Illinois no. 6 coal in ionic liquids, *Energy Fuels*, 2012, **26**, 3548–3552, DOI: 10.1021/ef3002923.

28 W. Q. Zhang, S. G. Jiang, K. Wang, L. Y. Wang, Z. Y. Wu, L. W. Kou and X. R. Ju, Study on coal spontaneous combustion characteristic structures affected by ionic liquids, *Procedia Eng.*, 2011, **26**, 480–500, DOI: 10.1016/j.proeng.2011.11.2195.

29 L. Bai, Y. Nie, Y. Li, H. F. Dong and X. P. Zhang, Protic ionic liquids extract asphaltenes from direct coal liquefaction residue at room temperature, *Fuel Process. Technol.*, 2013, **108**, 94–100, DOI: 10.1016/j.fuproc.2012.04.008.

30 W. Q. Zhang, S. G. Jiang and Z. Y. Wu, Study of the effect ionic liquids have on hydrogen bonds of coal, *J. China Univ. Min. Technol.*, 2013, **42**, 200–205, DOI: 10.13247/j.cnki.jcumt.2013.02.007.

31 W. Q. Zhang, S. G. Jiang, K. Wang, Z. Y. Wu and H. Shao, An experimental study of the effect of ionic liquids on the low temperature oxidation of coal, *Int. J. Min. Sci. Technol.*, 2012, **22**, 687–691, DOI: 10.1016/j.ijmst.2012.08.016.

32 W. Q. Zhang, S. J. Jiang, K. Wang, L. Y. Wang, Z. Y. Wu, L. W. Kou and X. R. Ju, Study on coal spontaneous combustion characteristic structures affected by ionic liquids, *Procedia Eng.*, 2011, **26**, 480–485, DOI: 10.1016/j.proeng.2011.11.2195.

33 F. S. Cui, B. L. Wang, C. M. Shu and J. C. Jiang, Inhibiting effect of imidazolium-based ionic liquids on the spontaneous combustion characteristics of lignite, *Fuel*, 2018, **217**, 508–514, DOI: 10.1016/j.fuel.2017.12.092.

34 L. Y. Wang, Y. L. Xu, S. G. Jiang, M. G. Yu, T. X. Chu, W. Q. Zhang, Z. Y. Wu and L. W. Kou, Imidazolium based ionic liquids affecting functional groups and oxidation properties of bituminous coal, *Saf. Sci.*, 2012, **50**, 1528–1534, DOI: 10.1016/j.ssci.2012.03.006.

35 J. Deng, Z. J. Bai, Y. Xiao, B. L. Wang, C. M. Shu and C. P. Wang, Thermogravimetric analysis of the effects of four ionic liquids on the combustion characteristics and kinetics of weak caking coal, *J. Mol. Liq.*, 2019, **277**, 876–885, DOI: 10.1016/j.molliq.2019.01.004.

36 J. W. Kim, D. Kim, C. S. Ra, G. B. Han, N.-K. Park, T. J. Lee and M. Kang, Synthesis of ionic liquids based on alkyl imidazolium salts and their coal dissolution and dispersion properties, *J. Ind. Eng. Chem.*, 2014, **20**, 372–378, DOI: 10.1016/j.jiec.2013.04.039.

37 P. Painter, N. Pulati, R. Cetiner, M. Sobkowiak, G. Mitchell and J. Mathews, Dissolution and dispersion of coal in ionic liquids, *Energy Fuels*, 2010, **24**, 1322–1335, DOI: 10.1021/ef9013955.

38 P. Painter, R. Cetiner, N. Pulati, M. Sobkowiak and J. Mathews, Dispersion of liquefaction catalysts in coal using ionic liquids, *Energy Fuels*, 2010, **24**, 3086–3092, DOI: 10.1021/ef100158v.

39 C. L. Song, X. R. Liu, S. S. Zhao and Z. W. Yang, Flame retardancy of anion in Imidazoles ionic liquids on Xinjiang lignite, *J. China Coal Soc.*, 2020, **11**, 60–65, DOI: 10.13225/j.cnki.jccs.2019.1681.

40 J. N. Xie, G. H. Ni, H. C. Xie, S. Li, Q. Sun and K. Dong, The effect of adding surfactant to the treating acid on the chemical properties of an acid-treated coal, *Powder Technol.*, 2019, **356**, 263–272, DOI: 10.1016/j.powtec.2019.08.039.

41 F. Yang, Y. C. Hou, S. H. Ren and W. Z. Wu, Selective oxidation of lignite to carboxyl chemicals, *Sci. Sin.: Chim.*, 2018, **48**, 574–589.

42 J. Deng, Z. J. Bai, Y. Xiao, C. M. Shu and B. L. Wang, Effects of imidazole ionic liquid on macroparameters and microstructure of bituminous coal during low-temperature oxidation, *Fuel*, 2019, **246**, 160–168, DOI: 10.1016/j.molliq.2019.01.004.

43 Z. Li, G. H. Ni, L. L. Sun, Q. Sun, S. Li, K. Dong, J. N. Xie and W. Gang, Effect of ionic liquid treatment on pore structure and fractal characteristics of low rank coal, *Fuel*, 2020, **262**, 116513, DOI: 10.1016/j.fuel.2019.116513.

44 B. Sanjukta, M. Kaustubha and B. Tamal, Quantum chemical insights and continuum solvation predictions on the dissolution of bituminous and anthracite coal in Ionic Liquid, *J. Mol. Liq.*, 2016, **221**, 919–929, DOI: 10.1016/j.molliq.2016.06.042.

45 X. Q. He, X. F. Liu, B. S. Nie and D. Z. Song, FTIR and Raman spectroscopy characterization of functional groups in various rank coal, *Fuel*, 2017, **206**, 555–563, DOI: 10.1016/j.fuel.2017.05.101.

46 J. Y. Jiang, W. H. Yang, Y. P. Cheng, Z. D. Liu, Q. Zhang and Z. Ke, Molecular structure characterization of middle-high rank coal *via* XRD, Raman and FTIR spectroscopy:Implications for coalification, *Fuel*, 2019, **239**, 559–572, DOI: 10.1016/j.fuel.2018.11.057.

47 L. Chen, C. Wen, W. Wang, T. Liu, E. Liu, H. Liu and Z. Li, Combustion behaviour of biochars thermally pretreated *via* torrefaction, slow pyrolysis, or hydrothermal carbonisation and co-fired with pulverised coal, *J. Renewable Energy*, 2020, **161**, 867–877, DOI: 10.1016/j.renene.2020.06.148.

48 X. Liu, L. Feng, L. Song, X. Wang and Y. Zhang, Effect of NaOH treatment on combustion performance of Xilinhaote lignite, *Int. J. Min. Sci. Technol.*, 2014, **24**, 51–55, DOI: 10.1016/j.ijmst.2013.12.009.

49 Th. Damartzis, D. Vamvuka, S. Sfakiotakis and A. Zabaniotou, Thermal degradation studies and kinetic Modeling of cardoon (Cynara Cardunculus) pyrolysis using thermogravimetric analysis(TGA), *Bioresour. Technol.*, 2011, **102**, 6230–6238, DOI: 10.1016/j.biortech.2011.02.060.

50 H. P. Lv, B. Li, J. Deng, L. L. Ye, W. Gao, C. M. Shu and M. S. Bi, A novel methodology for evaluating the inhibitory effect of chloride salts on the ignition risk of coal spontaneous combustion, *Energy*, 2021, **231**, 121093, DOI: 10.1016/j.energy.2021.121093.

51 S. N. Aki, J. F. Brennecke and A. Samanta, How polar are room-temperature ionic liquids?, *Chem. Commun.*, 2001, **11**, 413–414, DOI: 10.1039/b008039j.

52 X. Xi, Q. Shi, S. Jiang, W. Zhang, K. Wang and Z. Wu, Study on the effect of ionic liquids on coal spontaneous combustion characteristic by microstructure and thermodynamic, *Process Saf. Environ.*, 2020, **140**, 190–198, DOI: 10.1016/j.psep.2020.05.003.

53 X. Li, F. G. Zeng, W. Wang and K. Dong, XRD characterization of structural evolution in low-middle rank coals, *J. Fuel Chem. Technol.*, 2016, **44**, 777–783.

54 B. Wang, Y. J. Peng and S. Vink, Diagnosis of the surface chemistry effects on fine coal flotation using saline water, *Energy Fuels*, 2013, **27**, 4869–4874, DOI: 10.1021/ef400909r.

55 W. C. Xia, J. G. Yang and C. Liang, Investigation of changes in surface properties of bituminous coal during natural weathering processes by XPS and SEM, *Appl. Surf. Sci.*, 2014, **293**, 293–298, DOI: **10.1016/j.apsusc.2013.12.151**.

56 J. L. Song, J. Liang, X. M. Liu, W. E. Krause, J. P. Hinestroza and O. J. Rojas, Development and characterization of thin polymer films relevant to fiber processing, *Thin Solid Films*, 2009, **517**, 4348–4354, DOI: **10.1016/j.tsf.2009.03.015**.

57 H. Z. Chang, C. G. Wang, F. G. Zeng, J. Li, W. Y. Li and K. C. Xie, XPS comparative analysis of coal macerals with different reducibility, *J. Fuel Chem. Technol.*, 2006, **34**, 389–394, DOI: **10.3969/j.issn.0253-2409.2006.04.002**.